ARTICLE

Efficient 1-(thiophen-2-yl)isoquinoline-based ionic iridophosphors with bulky counterion for solution-processed deep-red electroluminescence

Peng Tao,*[a,b] Xiao-Kang Zheng,[a] He Jiang,[a] Xinghao Sheng,[a] Yongjing Deng,[c] Yuk Yin Ian Chan,[a] Qiang Zhao,*[c] and Wai-Yeung Wong*[a,b]

A pair of high-efficiency deep-red emissive ionic iridophosphors (**Ira** and **Irb**) showing high photoluminescence quantum yields (PLQYs) are rationally designed by using 1-(thiophen-2-yl)isoquinoline as the cyclometalating ligand. Two bulky tetraarylborate anions (tetraphenylborate and tetrakis(3,5-bis(trifluoromethyl)phenyl)borate) are selected to improve their PLQYs in both solution and aggregated state, which enables the efficient electroluminescence *via* solution-processed approach. The variation of the tetraarylborate anions also aims to tune the photophysical properties of these deep-red emissive iridophosphors. Both ionic iridophosphors emit intense deep-red room-temperature phosphorescence in both solution and aggregated states. The phosphorescence spectra of both complexes are similar (630 nm with a shoulder emission of 686 nm) in CH_2Cl_2, originating from the same cation species of the complexes. Both complexes show high PLQYs in CH_2Cl_2 (0.41 for **Ira**, 0.43 for **Irb**) and neat film (0.27 for **Ira**, 0.34 for **Irb**). Moreover, they serve as the triplet emitters to evaluate their performance in the solution-processed deep-red electroluminescent devices. The maximum external quantum efficiencies for the deep-red electroluminescence are 7.3% with emission maximum of 649 nm for **Ira**, and 10.2% with emission maximum of 635 nm for **Irb**, respectively, implying that they are the good candidates for high-performance electroluminescence.

1. Introduction

Luminescent materials can be classified as the neutral and ionic species according to their nature of charge.[1-3] Recently, the ionic luminescent materials are emerging as an appealing category of new photofunctional materials owing to their flexible molecular design on both cation and anion parts, which are widely involved in many fields, for instance, information recording and security protection, biosensing and bioimaging, photodynamic therapy as well as organic light-emitting diodes (OLEDs).[4-8] Different from the neutral luminescent materials, the ionic ones consist of cation part and anion part *via* electrostatic interactions. Thus, the excited states of these ionic luminescent materials could be tuned independently by their structural design of the cation or anion.[9-12] Among the ionic luminescent materials, the luminescent ionic transition-metal complexes represent one of the competitive alternatives attributed to their appealing excited states (*e.g.*, efficient photoluminescence (PL), tunable energy in emission, and controllable emissive lifetime, *etc*).[13-16] The luminescent ionic iridophosphors would be the ideal candidates for such kind of materials, especially for their full exciton utilization ability in the OLEDs, remarkably boosting the device performance.[13,15,16] Since the first dry-processed OLEDs based on ionic iridophosphors were demonstrated by us,[13] the ionic iridophosphors have become the research focus in this area.[13,16] In spite of many kinds of ionic iridophosphors have been developed, there are still limited examples compared to the neutral ones.[3] Also, the research studies focusing on the ionic iridophosphors for electroluminescence are quite restricted.[3,13,15,16]

In general, the counterions usually play vital roles in manipulating the properties of the ionic iridophosphors.[12,16] Taking cationic iridophosphor as an example, it was found that the sublimabilities of these complexes are highly dependent on the volume of the anions.[12] Increasing the volume of anion (*e.g.*, from hexafluorophosphate to tetraphenylborate) can remarkably enhance their PL quantum yields (PLQYs) in aggregated state, thereby resulting in the improved device performance.[13,16] Another important influence of the anion is on their emission spectra in aggregated state. The bulky anions can effectively prevent the phosphorescence quenching from the triplet-triplet annihilation and inhibit the π-π interactions of the iridium(III) cations, generating the high PLQYs and maintaining the unimolecular emission feature similar to that in solution state.[16] The emission energies of the cationic iridophosphors are mainly determined by their cyclometalating ligands. Currently, the majority of the reported examples of

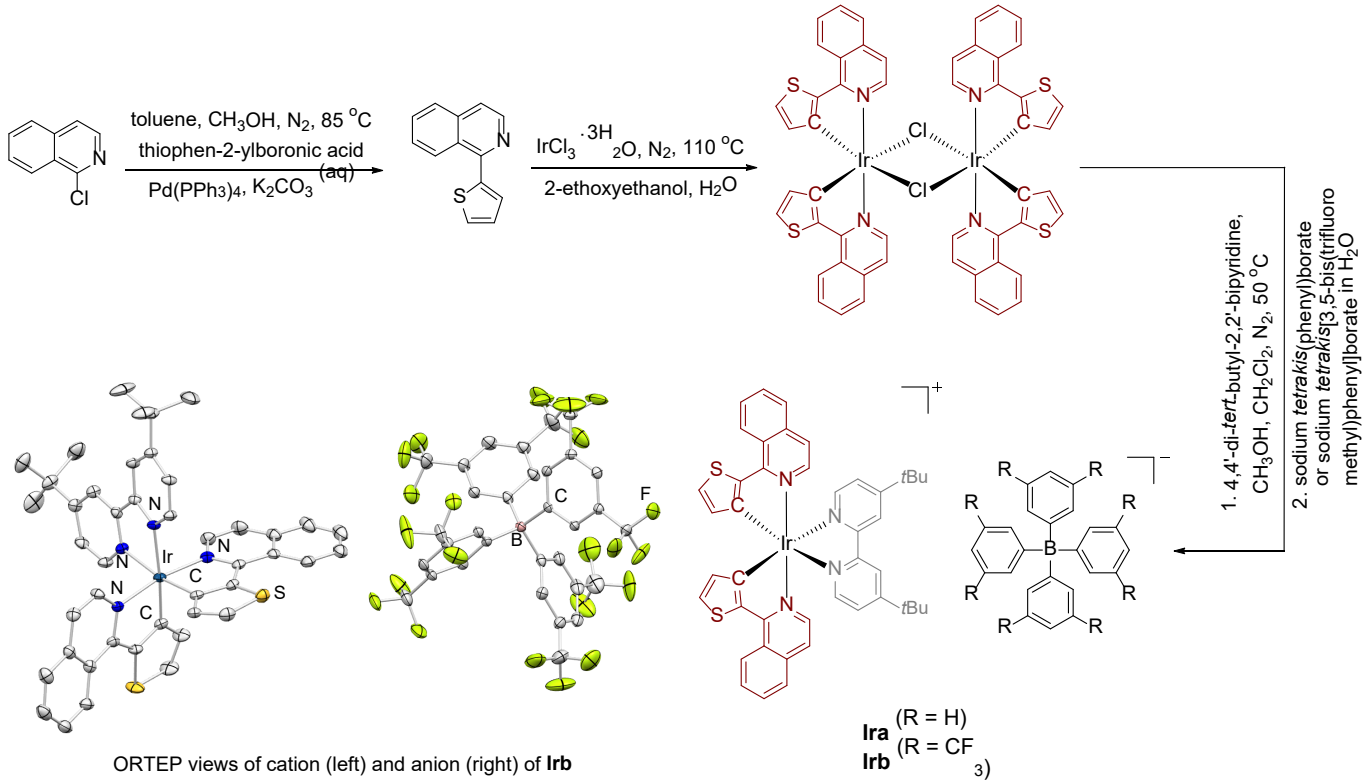

Scheme 1. The molecular structures and synthesis of the new deep-red emissive ionic iridophosphors, and ORTEP view of **Irb** (CCDC no. 2203809). The hydrogen atoms and solvent molecule are omitted for clarity.

ionic iridophosphors for electroluminescence are green or yellow emissive.[13,15-18] Recently, we developed a pair of efficient yellow emissive cationic iridium(III) complexes by using chlorine functionalized 2-phenylquinoline derivative as the cyclometalating ligand and selecting the bulky trifluoromethyl functionalized tetraphenylborate as the counterion, achieving high peak external quantum efficiency (EQE) of 11.6% by dry-processed method.[18] Duan and coworkers also realized highly efficient yellow electrophosphorescence with a peak EQE of 15.8% by incorporating a new ionic iridophosphor as the emitter.[17] However, high-efficiency blue and red electroluminescence based on ionic iridophosphors are extremely rare,[19] which will further hinder their applications in solid-state lighting as well as full colour displays. Very recently, a 2,3-diphenylquinoxaline-based deep-red emissive ionic iridophosphor was designed for OLEDs by Ma *et al.*, and an electroluminescence (λ_{EL} = 632 nm) with high colour purity was obtained with a peak EQE of 10.3%.[19] The red/deep-red emitters usually suffer from the energy-gap law, resulting in the low efficiency in photoluminescence.[20] Thus, it is necessary to further explore the new pure-red/deep-red ionic iridophosphors with high efficiency for electroluminescence.

In this work, a pair of new deep-red emissive ionic iridophosphors (**Ira** and **Irb**) were well designed by choosing 1-(thiophen-2-yl)isoquinoline and 4,4'-di-*tert*-butyl-2,2'-bipyridine as the cyclometalating and ancillary ligands (**Scheme 1**). Two bulky tetraarylborate served as the counterions to tune their photophysical properties. The ionic phosphors obtained show bright deep-red phosphorescence (630 nm with 686 nm as the shoulder emission) with high PLQYs (0.41 for **Ira**, 0.43 for **Irb**) in solution beneficial to the electroluminescence. Two iridophosphors were further used as the triplet emitters, affording the maximum current efficiency (CE), power efficiency (PE), and EQE for solution-processed deep-red OLEDs of 3.50 cd/A, 2.05 lm/W, and 7.3% for **Ira** (emission maximum of 649 nm), and 4.02 cd/A, 1.57 lm/W, and 10.2% for **Irb** (emission maximum of 636 nm), respectively.

2. Results and discussion

2.1 Synthesis and characterizations

Scheme 1 shows the synthesis of the new ionic iridophosphors. The ligand 1-(thiophen-2-yl)isoquinoline was prepared in high yield *via* the Suzuki carbon-carbon coupling reaction. The iridium(III) dimer complex was synthesized by heating $IrCl_3·3H_2O$ with 1-(thiophen-2-yl)isoquinoline ligand in the solvent mixture of H_2O and 2-eyhoxyethanol under N_2 at 110 °C.[21] The target ionic complexes were prepared by two steps. Firstly, the iridophosphors containing chloride as the counterion were obtained by stirring ancillary ligand 4,4'-di-*tert*-butyl-2,2'-bipyridine with the iridium(III) dimer in CH_2Cl_2 at 50 °C under N_2. Secondly, the two complexes were prepared *via* counterion exchange reaction and purified by column chromatography (eluent: CH_2Cl_2; stationary phase: silica gel) to give brown powders.[18] Both iridophosphors were characterized and confirmed by mass spectrometry (MS) and nuclear magnetic resonance (NMR) spectrometry. Due to the same chemical environment of the two cyclometalated ligands of **Ira** and **Irb** induced by the symmetric 4,4'-di-*tert*-butyl-2,2'-bipyridine ligand, the proton resonance signals from each cyclometalated ligand overlap perfectly

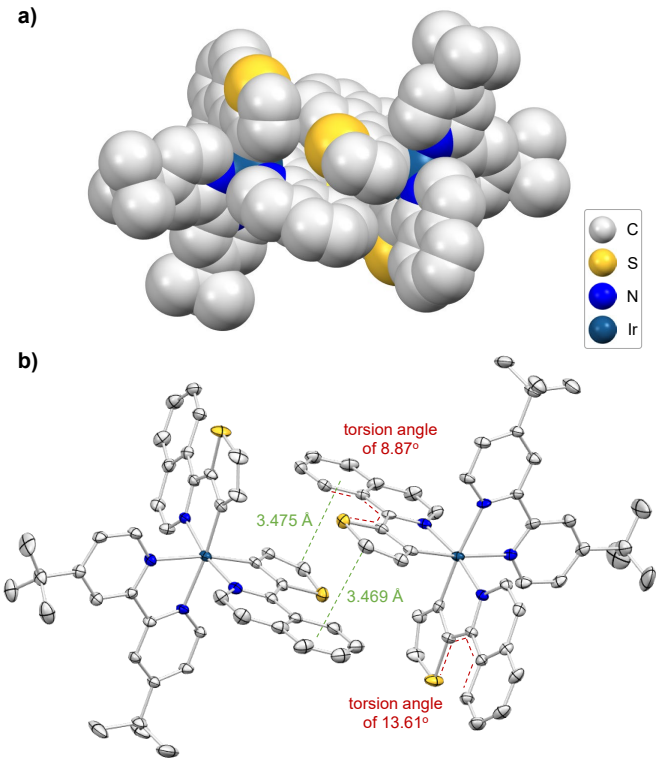

Figure 1. The spacefill view (a) and ORTEP view (b) for the π-π interaction between the adjacent iridium(III) cations and the torsion angles in the cyclometalated ligands of **Irb** in crystal state.

with the signals from another, which is similar to the reported heteroleptic iridophosphors bearing symmetric ancillary ligand.[18] Only one singlet resonance signal was observed from the $^{19}F\{^{1}H\}$ NMR spectrum for **Irb**, indicating the bulky tetraarylborate was successfully introduced to form the target ionic iridophosphor. Owing to the incorporation of the lipophilic trifluoromethyl groups into the tetraarylborate anion, complex **Irb** exhibits much higher solubility than that of **Ira** in common organic solvents (*e.g.*, CH_2Cl_2).

The block crystals of **Irb** were cultivated *via* the slow evaporation of the mixed solvents (CH_2Cl_2 and methanol). The crystal structure of **Irb** was undoubtedly confirmed by the single crystal X-ray diffraction. The Oak Ridge thermal ellipsoid plot (ORTEP) views of the iridium(III) cation and the bulky tetraarylborate anion of **Irb** are shown in **Scheme 1**. Similar to the reported examples, a slightly distorted octahedral configuration is adopted by iridium(III) centre, where the nitrogen atoms from the cyclometalated ligands adopt *trans* coordination configuration and the coordinated carbon atoms adopt *cis* configuration.[17,18] As depicted in **Figure 1b**, the small torsion angles (8.87° and 13.61°) between the isoquinoline unit and thiophene moiety were observed because of the less repulsion between the sulphur atom and hydrogen atom from the isoquinoline unit. Moreover, there exists an evident π-π interaction between the adjacent iridium(III) cations (**Figure 1**), and the distance of the π-π interaction was determined to be around 3.47 Å, suggesting the presence of the strong intermolecular interactions in crystal state.

2.2 Photophysical properties

The photophysical properties of the as-prepared iridophosphors were then investigated in both solution and neat film. As shown in **Figure 2**, the absorption and luminescent properties of two iridophosphors were explored at 1.0×10^{-5} mol/L in CH_2Cl_2 and neat film at room temperature. The phosphorescence spectra at low-temperature (77 K) were measured in CH_2Cl_2 (**Figure 3a**). Although a slight difference exists in the counterions of complexes **Ira** and **Irb**, both complexes show almost the same absorption spectra (**Figure 2**). As summarized in **Table S1**, for both complexes, they absorb at 225, 306, 347, 390, and 480 nm. The $^{1}\pi\rightarrow\pi^{*}$ transition from the cyclometalated ligands of the iridophosphors is responsible for the strong absorption ranging from 220 nm to 400 nm.[13] The relatively weak absorption ranging from 400 nm to 510 nm could be attributed to the metal-to-ligand charge-transfer of iridophosphors.[13] At room temperature, under the excitation of near-ultraviolet light of 400 nm, both ionic iridophosphors show the same emission spectra in CH_2Cl_2 and emit intense deep-red phosphorescence peaking at 630 nm (686 nm as the emission shoulder) (**Figure 2**). Owing to the high intensities of the emission shoulders, both complexes show broad full width at half maxima (FWHM) of about 92 nm (**Table 1**). The deep-red phosphorescence of two iridophosphors from the low triplet excited state is the result of the strong interaction of the 1-(thiophen-2-yl)isoquinoline ligand with the iridium(III) ion.[18] Compared to their 1-phenylisoquinoline-based analogues (λ_{PL} = ~593 nm), the replacement of the phenyl moiety of 1-phenylisoquinoline ligand

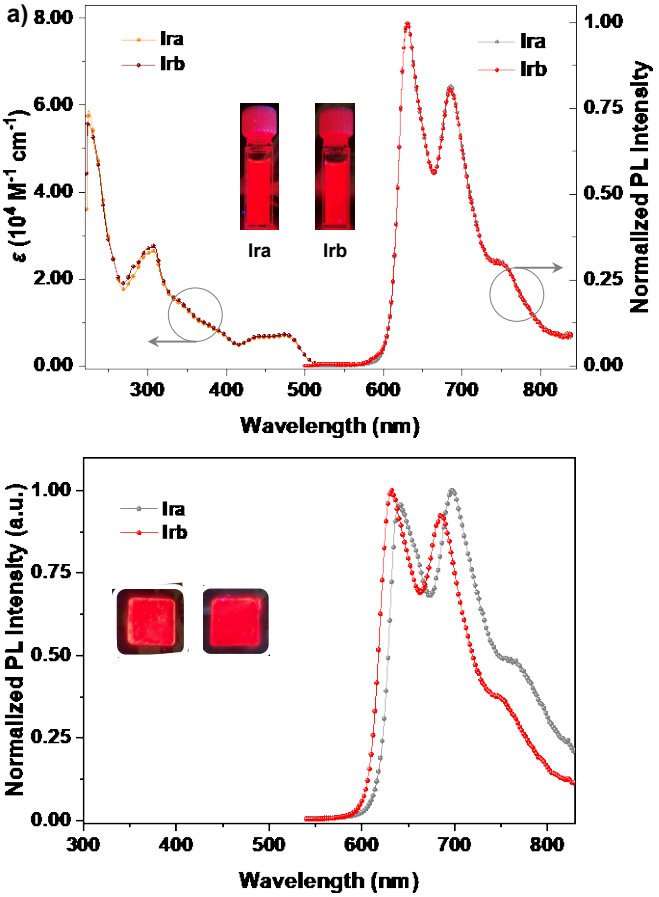

Figure 2. a) The UV-visible absorption spectra and PL spectra of **Ira** and **Irb** at 1.0×10^{-5} mol/L in CH_2Cl_2 at 298 K (ε refers to the molar extinction coefficient, λ_{ex} = 365 nm); b) PL spectra of **Ira** and **Irb** in neat film at 298 K (λ_{ex} = 365 nm). Inset: The photographs of two emitters in CH_2Cl_2 (a) or in neat film (b) under UV light of 365 nm.

Table 1. Photophysical and electrochemical properties of deep-red ionic iridophosphors.

Complex	Emission				E_{onset}^{ox} [c] [eV]	E_g [d] [eV]	T_1 [e] [eV]	HOMO/LUMO [d] [eV]
	λ_{em} [a] [nm]	FWHM [nm]	τ [b] [μs]	PLQY				
Ira	630, 686 (sh)	92	1.16	0.41	0.81	1.97	1.97	-5.61/-3.64
Irb	630, 686 (sh)	92	1.51	0.43	0.81	1.97	1.97	-5.61/-3.64

[a]At 1.0 × 10^{-5} mol/L in O_2-free CH_2Cl_2 at 298 K, λ_{ex} = 365 nm, sh refers to the shoulder emission; [b]λ_{ex} = 375 nm; [c]In CH_3CN under Ar; [d]HOMO (eV) = -e(E_{onset}^{ox} + 4.8), E_g = 1240/λ, LUMO (eV) = E_g + HOMO; [e]Estimated from the highest-energy vibronic sub-band of the phosphorescence spectrum at 1.0 × 10^{-5} mol/L in CH_2Cl_2 at 77 K, λ_{ex} = 365 nm.

with thienyl unit results in a remarkable red-shift (37 nm) in emission peak induced by the more electron-rich nature of thienyl unit, which can be revealed by the variation in the calculated frontier molecular orbitals (see details in the section of Theoretical calculations).[17] The same emission spectra also demonstrated that the counterions have no influence on the emission energy of two ionic iridophosphors in solution. The PLQYs of two deep-red iridophosphors in O_2-free CH_2Cl_2 are 0.41 for **Ira** and 0.43 for **Irb** at room temperature, which is higher than that of their 1-phenylisoquinoline-based analogue (Φ_{PL} = 0.32).[17] Furthermore, both ionic iridophosphors show relatively short phosphorescence lifetimes in O_2-free CH_2Cl_2 (1.16 μs for Ira, 1.51 μs for Irb) at room temperature (Figure 3b).

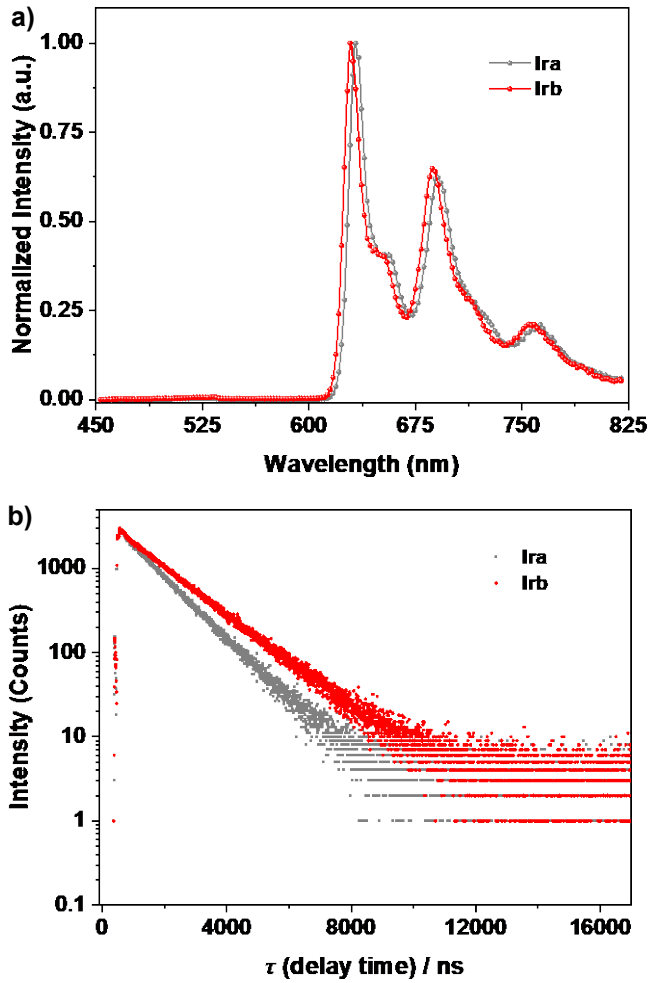

Figure 3. a) PL spectra of **Ira** and **Irb** at 1.0 × 10^{-5} mol/L in CH_2Cl_2 at 77 K (λ_{ex} = 365 nm); b) Delay time of **Ira** and **Irb** at 1.0 × 10^{-5} mol/L in O_2-free CH_2Cl_2 at 298 K (λ_{ex} = 375 nm).

Both complexes also show intense deep-red phosphorescence in neat film at room temperature. The phosphorescence of both iridophosphors in neat film also exhibits structured emission similar to those in solution state (**Figure 2b**). Notably, in spite of the presence of the π-π interaction in crystal state, the emission of **Irb** (λ_{PL} = 631 nm with 685 nm as the emission shoulder) is almost the same as that in CH_2Cl_2 (**Table S2**), implying the absence of the π-π interaction in neat film. In contrast, complex **Ira** only shows slightly red-shifted emission and emits at 641 nm with 697 nm as the emission shoulder (**Table S2**), which is probably induced by the weak intermolecular interaction in neat film. The slight difference in emission can be attributed to the different counterions present in the complexes. An explanation for the differential behavior could be proposed as follows. Because of the size difference in the counterions of two complexes, the complex **Irb** with CF_3-bearing counterion (larger in size) tends to form the amorphous state owing to the fast evaporation of the solvent during spin-coating. The complex **Ira** with smaller counterion may form some weak intermolecular interaction (*e.g.*, π-π interaction) in neat film. As listed in **Table S2**, two complexes show much shorter phosphorescence lifetimes (τ_1 = 0.12 μs (6%), τ_1 = 0.56 μs (94%) for **Ira**; τ_1 = 0.31 μs (19%), τ_1 = 0.85 μs (81%) for **Irb**) in neat film than those in O_2-free CH_2Cl_2, which may be due to the increased non-radiative decay rate for the complexes in neat film.[22] Attributed to the suppressed triplet-triplet annihilation by the bulky counterions, both complexes also give high PLQYs (0.27 for **Ira**, 0.34 for **Irb**) in neat film, thereby suggesting that they are the good candidates for electroluminescence.

The triplet excited states (T_1) for both complexes are determined by their 77 K-phosphorescence spectra in CH_2Cl_2. The low-temperature spectra exhibit fine structures with vibronic bands peaking at 630 nm (with 688 nm as the shoulder emission) for both complexes, and the emission maxima are almost the same to those at 298 K (**Figure 3a**). The energy levels of T_1 for both deep-red complexes were estimated to be 1.97 eV according to the low-temperature spectra.[17]

2.3 Electrochemical properties

The electrochemical properties of two ionic iridophosphors were explored by cyclic voltammetry (CV) in CH_3CN under Ar. **Figure S1** shows the CV curves of two iridophosphors. Considering the same iridium(III) cation for both complexes, the reversible oxidation wave at almost the same potential should be assigned to the oxidation process on the iridium(III) centre, and the onset potentials in

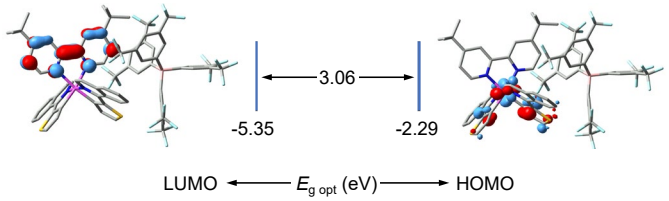

Figure 4. The calculated electron cloud distributions, energy levels, and $E_{g\ opt}$ of LUMO and HOMO for **Irb** at the ground state.

oxidation were estimated to be 0.81 V for both complexes.[18] However, after ruling out the possible interferences, one irreversible oxidation was still only observed for complex **Ira**, which cannot be well assigned at present. According to the CV curves, the energy levels of the lowest unoccupied molecular orbitals (LUMO) and the highest occupied molecular orbital (HOMO) of both deep-red iridophosphors were calculated to be -5.61 and -3.64 eV, respectively.[17]

2.4 Theoretical calculations

The time-dependent density functional theory (TD-DFT) calculations were then carried out for complex **Irb** to get a deep insight into their photophysical properties. TD-DFT calculations were conducted with the B3LYP functional theory. The LanL2DZ basis set was used for iridium atom, while the 6-31G(d,p) basis set was employed for carbon, hydrogen, nitrogen, oxygen, sulfur and fluorine atoms.[23] As shown in **Figure 4**, at the ground state, the calculated electron clouds of LUMO and HOMO for **Irb** are distributed over the iridium(III) cation, and there is no electron cloud distributed over the tetrakis(3,5-bis(trifluoromethyl)phenyl)borate anion, implying that the bulky anion does not contribute to the excited state of complex **Irb**. The electron clouds of HOMO mainly distribute over the cyclometalated ligands and iridium center, while the electron clouds of LUMO mainly distribute over the 4,4'-di-*tert*-butyl-2,2'-bipyridine ancillary ligand. The results are consistent with the reported analogues.[18,24] The calculated energy levels of LUMO, HOMO, and $E_{g\ opt}$ for **Irb** at the ground state are -5.35 eV, -2.29 eV, and 3.06 eV, respectively.

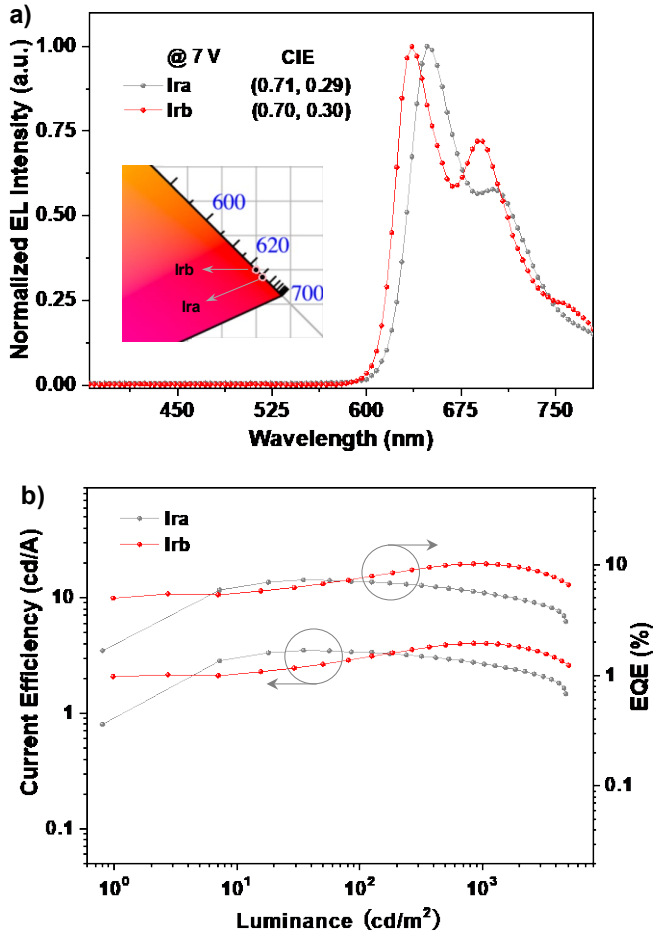

Figure 5. EL spectra (a) and CE-L-EQE curves (b) of the devices based on **Ira** and **Irb** (inset: 1931 CIE coordinates under 7 V).

2.5 Deep-red phosphorescent electroluminescence

Finally, two deep-red ionic iridophosphors were used as the dopants to further evaluate their device performance in the deep-red electroluminescence. The deep-red OLEDs were designed with the configurations as below: indium tin oxide (ITO)/modified poly(3,4-ethylenedioxythiophene) polystyrene sulfonate (*m*-PEDOT:PSS) (70 nm)/*bis*[2-(2-hydroxyphenyl)-pyridine]beryllium ($Bepp_2$): 6 wt% of **Ira** or **Irb** (40 nm)/2,2',2''-(1,3,5-benzinetriyl)-*tris*(1-phenyl-1-*H*-benzimidazole) (TPBi) (50 nm)/lithium fluoride (LiF) (1 nm)/aluminium (Al) (100 nm), where indium tin oxide is anode, *m*-PEDOT:PSS serves as the hole injection layer (HIL), and TPBi serves as the hole transport layer (HTL), respectively. $Bepp_2$ in the light-emitting layer (EML) acts as the host material for the two iridophosphors.[25] Considering the larger molecular weight of emitters, the increased doping concentration of 6 wt% for complexes was selected to ensure the complete energy transfer from the host to the iridium(III) cation. The hole injection layer and light-emitting layer were prepared by solution-processed method. The device structures and the energy levels of the functional materials involved, **Ira**, and **Irb**, are shown in **Figure S2**.

The device performances for **Ira** and **Irb** are shown in **Figures S3** and **5**. Both devices exhibit the turn-on voltage of 4.5 V and emit intense electrophosphorescence peaking at 649 nm with a shoulder emission of 703 nm for **Ira**, and 636 nm with a shoulder emission of 690 nm for **Irb** (**Figure 5a**). The 1931 Commission Internationale de l'Elcairage (CIE) coordinates of two OLEDs are (0.71, 0.29) and (0.70, 0.30), indicating the deep-red electroluminescence. Compared to the photoluminescence of complexes in solution, both devices exhibit slight red-shift in the emission maxima of the electroluminescence, which could be probably originated from the intermolecular π-π interactions between the iridium(III) cations and the $Bepp_2$ host. From the energy level diagram of the OLEDs (**Figure S2**), the LUMO and HOMO levels of **Ira** and **Irb** are all within those of the $Bepp_2$ host, and the triplet energy level of the $Bepp_2$ host is higher than those of the two complexes, suggesting the good carrier trapping in the light-emitting layers.[25,26] No residual emission from the $Bepp_2$ host was observed, proving that the complete energy transfer from the $Bepp_2$ host to the iridium(III) cations occurred in these devices.[25,26]

As depicted in **Figures 5b** and **S3**, the maximum brightness of the devices based on **Ira** and **Irb** are 4,792 and 5,046 cd/m^2, respectively. The peak power efficiencies, current efficiencies, and external quantum efficiencies are 2.05 lm/W, 3.50 cd/A, and 7.3% for **Ira**, and 1.57 lm/W, 4.02 cd/A, and 10.2% for **Irb**, respectively. The device performance of **Irb** is much higher than that of **Ira**, demonstrating

that the incorporation of the trifluoromethyl groups into the tetraarylborate anion has a great influence (*e.g.*, suppression of the triplet−triplet annihilation effect) on the enhancement of the device performance. The peak EQE for **Irb** is comparable to the best result reported recently for the ionic iridophosphors in the deep-red region.[19] The electroluminescence performance of these ionic iridophosphors could be further improved by selecting other suitable host materials or optimizing the device structure.

3. Conclusions

In summary, by incorporating 1-(thiophen-2-yl)isoquinoline as the cyclometalating ligand and bulky tetraarylborate anions as the counterions, a pair of new high-efficiency deep-red ionic iridophosphors are designed rationally. At room temperature, both iridophosphors emit bright deep-red phosphorescence (630 nm with a shoulder emission of 686 nm for both complexes), and high PLQY (0.41 for **Ira**, 0.43 for **Irb**) in CH_2Cl_2, and they show slight difference in emission, which could be attributed to the different counterions present in the complexes. The replacement of the phenyl moiety of 1-phenylisoquinoline ligand with thienyl unit results in the remarkable red-shift in emission, which is the result of the more electron-rich nature of thienyl unit. Two ionic iridophosphors were further used as the triplet emitters for the solution-processed deep-red electroluminescence, and the peak EQE of 10.2% is realized for the deep-red OLED based on **Irb** with the electroluminescence peaking at 636 nm. Although the prepared devices show lower performance than the state-of-the-art deep-red OLEDs based on neutral iridium(III) complexes, it is believed that the device performance based on ionic iridium(III) emitters will be improved by further molecular design.

4. Experimental

The additional information on the characterizations, OLED fabrication, MS, and NMR spectra can be found in Electronic Supplementary Information.

4.1 Synthesis of 1-(thiophen-2-yl)isoquinoline

Thiophen-2-ylboronic acid (5.5 mmol), 1-chloroisoquinoline (5 mmol), $Pd(PPh_3)_4$ (0.3 mmol), toluene (60 mL), methanol (10 mL), and 2.0 M K_2CO_3 aqueous solution (10 mL) were heated under N_2 at 85 °C for 24 h. After completing the reaction, the solvent was evaporated, and the mixture was dissolved in CH_2Cl_2 and washed with water, and dried over anhydrous Na_2CO_3. The crude product was purified by column chromatography to give the product as a white powder (ethyl acetate and hexane as the eluent, v:v = 80:1) (88% Yield). ^{1}H NMR (400 MHz, chloroform-*d*) δ 8.57 (d, *J* = 5.7 Hz, 1H), 8.54 (d, *J* = 8.5 Hz, 1H), 7.89 (d, *J* = 8.2 Hz, 1H), 7.72 (t, *J* = 7.1 Hz, 1H), 7.65 – 7.60 (m, 3H), 7.55 (d, *J* = 5.1 Hz, 1H), 7.23 (dd, *J* = 5.0, 3.7 Hz, 1H). ^{13}C{^{1}H} NMR (101 MHz, chloroform-*d*) δ 153.56, 142.82, 142.16, 137.10, 130.13, 128.74, 127.97, 127.67, 127.47, 127.21, 126.85, 126.21, 119.92. HRMS (ESI) m/z: $[M+H]^+$ calcd for $C_{13}H_{10}NS^+$, 212.0534; found, 212.0534.

4.2 Synthesis of deep-red emissive ionic iridophosphors

The iridium(III) dimer complex was prepared as a red powder by reacting $IrCl_3{\cdot}3H_2O$ with 1-(thiophen-2-yl)isoquinoline in the solvent mixture of water and 2-eyhoxyethanol (v:v = 1:3) at 110 °C under N_2. The dimer complex (0.2 mmol) together with 4,4'-di-*tert*-butyl-2,2'-bipyridine (0.44 mmol) were added to the solution of CH_2Cl_2 (30 mL) and methanol for stirring under N_2 at 50 °C for 12 h. After completing the reaction, the mixed solvents were removed by rotary evaporator, and the crude iridium(III) intermediate was dissolved in methanol (20 mL). Sodium tetrakis(phenyl)borate (0.4 mmol) or sodium tetrakis[3,5-*bis*(trifluoromethyl)phenyl]borate (0.4 mmol) was dissolved in water (10 mL). Finally, the target ionic iridium(III) complexes can be precipitated by injecting the sodium tetraarylborate solution into the methanol solution containing crude iridium(III) intermediate. The crude product was finally purified to give the target ionic complexes by column chromatography using CH_2Cl_2 as eluent. The purity of the prepared complexes suitable for device fabrication was further improved by recrystallization for three times.

Ira. Brown powder (73% Yield). ^{1}H NMR (400 MHz, methylene chloride-d_2) δ 8.90 (d, *J* = 8.3 Hz, 2H), 8.27 (d, *J* = 1.7 Hz, 2H), 7.88 – 7.76 (m, 8H), 7.62 (d, *J* = 4.9 Hz, 2H), 7.46 (dd, *J* = 5.9, 1.8 Hz, 2H), 7.39 – 7.30 (m, 10H), 7.19 (d, *J* = 6.5 Hz, 2H), 7.03 (t, *J* = 7.4 Hz, 8H), 6.87 (t, *J* = 7.2 Hz, 4H), 6.40 (d, *J* = 4.9 Hz, 2H), 1.42 (s, 18H). ^{13}C{^{1}H} NMR (101 MHz, methylene chloride-d_2) δ 164.99, 164.79, 164.30, 164.10, 163.81, 163.32, 158.44, 155.38, 150.99, 141.02, 136.70, 136.02, 135.89, 135.88, 130.10, 125.61, 125.59, 125.56, 125.53, 121.65, 35.62, 30.02. MALDI-TOF-MS (m/z): calcd for the cation of complex $C_{44}H_{40}IrN_4S_2$, 881.232; found, 881.245.

Irb. Brown powder (70% Yield). ^{1}H NMR (400 MHz, methylene chloride-d_2) δ 8.90 (d, *J* = 7.9 Hz, 2H), 8.26 (d, *J* = 1.6 Hz, 2H), 7.88 – 7.77 (m, 8H), 7.74 (s, 8H), 7.63 (d, *J* = 4.9 Hz, 2H), 7.57 (s, 4H), 7.49 (dd, *J* = 5.9, 1.8 Hz, 2H), 7.37 (d, *J* = 6.5 Hz, 2H), 7.20 (d, *J* = 6.5 Hz, 2H), 6.41 (s, 2H), 1.41 (s, 18H). ^{13}C{^{1}H} NMR (101 MHz, methylene chloride-d_2) δ 165.03, 164.15, 162.48, 161.99, 161.49, 161.00, 158.43, 155.41, 150.95, 140.99, 136.70, 136.03, 134.77, 133.12, 132.17, 130.08, 128.84 (qq, *J* = 31.3, 2.5 Hz), 128.76, 127.14, 126.74, 125.92, 124.35, 123.21, 120.56, 120.51, 119.12, 117.48 (septet, *J* = 3.5 Hz), 35.57, 29.90. ^{19}F{^{1}H} NMR (565 MHz, methylene chloride-d_2) δ -62.85. MALDI-TOF-MS (m/z): calcd for the cation of complex $C_{44}H_{40}IrN_4S_2$, 881.232; found, 881.256.

Conflicts of interest

There are no conflicts to declare.

Acknowledgements

The authors acknowledge the National Key R&D Program of China (2022YFE0104100), National Natural Science Foundation of China (61905120), Start-up Fund for RAPs under the Strategic Hiring Scheme (P0035922), ITC Guangdong-Hong Kong Technology Cooperation Funding Scheme (TCFS) (GHP/038/19GD), CAS-Croucher Funding Scheme for Joint Laboratories (ZH4A), the Hong Kong Research Grants Council (PolyU 153058/19P), the Hong Kong Polytechnic University (YXB8), Research Institute for Smart Energy (CDAQ), and Miss Clarea Au for the Endowed Professorship in Energy (847S) for financial support. We also gratefully acknowledge the support of the University Research Facility on Chemical and

Environmental Analysis (UCEA) of The Hong Kong Polytechnic University.

Notes and references

[1] Z. Chen, C.-L. Ho, L. Wang and W.-Y. Wong, *Adv. Mater.*, **2020**, *32*, 1903269.
[2] H. Imahori, Y. Kobori and H. Kaji, *Acc. Mater. Res.*, **2021**, *2*, 501.
[3] D. Ma, T. Tsuboi, Y.Qiu and L. Duan, *Adv. Mater.*, **2017**, *29*, 1603253.
[4] P. Tao, S.-J. Liu and W.-Y. Wong, *Adv. Opt. Mater.*, **2020**, *8*, 2000985.
[5] R. Bai, X. Meng, X. Wang and L. He, *Adv. Funct. Mater.*, **2020**, *30*, 1907169.
[6] R. Yu, Y. Song, K. Zhang, X. Pang, M. Tian and L. He, *Adv. Funct. Mater.*, **2022**, *32*, 2110623.
[7] K. Y. Zhang, Q. Yu, H. Wei, S. Liu, Q. Zhao and W. Huang, *Chem. Rev.*, **2018**, *118*, 1770.
[8] R. Bai, X. Meng, X. Wang and L. He, *Adv. Funct. Mater.*, **2021**, *31*, 2007167.
[9] P. Tao, X. Lü, G. Zhou and W.-Y. Wong, *Acc. Mater. Res.*, **2022**, *3*, 830.
[10] S. Guo, T. Huang, S. Liu, K. Y. Zhang, H. Yang, J. Han, Q. Zhao and W. Huang, *Chem. Sci.*, **2017**, *8*, 348.
[11] V. W.-W. Yam, *Nat. Synth.*, **2023**, *2*, 94.
[12] D. Ma, Y. Qiu and L. Duan, *Adv. Funct. Mater*., **2016**, *26*, 3438.
[13] W.-Y. Wong, G.-J. Zhou, X.-M. Yu, H.-S. Kwok and Z. Lin, *Adv. Funct. Mater*., **2007**, *17*, 315.
[14] V. W.-W. Yam, V. K.-M. Au and S. Y.-L. Leung, *Chem. Rev.*, **2015**, *115*, 7589.
[15] L. He, L. Duan, J. Qiao, D. Zhang, L. Wang and Y. Qiu, *Org. Electron*., **2010**, *11*, 1185.
[16] D. Ma, L. Duan, Y. Wei, L. He, L. Wang and Y. Qiu, *Chem. Commun*., **2014**, *50*, 530.
[17] D. Ma, R. Liu, C. Zhang, Y. Qiu and L. Duan, *ACS Photonics*, **2018**, *5*, 3428.
[18] P. Tao, X. Zheng, Y.-K. Lee, G.-L. Wang, F.-Y. Li, Z.-K. Li, Q. Zhao, Y.-Q. Miao and W.-Y. Wong, *Adv. Photonics Res.*, **2021**, *2*, 2100115.
[19] R. Liu, D. Ma and L. Duan, *J. Mater. Chem. C*, **2020**, *8*, 14766.
[20] (a) E. A. Katlenok, D. M. Kryukov, A. E. Kurtsevich, K. M. Degtyarenko, R. R. Valiev, O. V. Levin, V. Yu. Kukushkin and A. V. Rozhkov, *Inorg. Chem.*, **2023**, *62*, 11080; (b) C. Jiang, S. Yoon, Y. H. Nguyen and T. S. Teets, *Inorg. Chem.*, **2023**, *62*, 11278; (c) K. S. Bejoymohandas, H. U. Kim, S. Sohn, W. Choi, S. Jung, F. Monti and T. Park, *Inorg. Chem.*, **2023**, *62*, 43.
[21] M. Nonoyama, *Chem. Soc. Jpn.*, **1974**, *47*, 767.
[22] Y. Jian, S. Peng, X. Li, X. Wen, J. He, L. Jiang and Y. Dang, *Inorg. Chim. Acta*, **2011**, *368*, 37.
[23] M. J. Frisch, *et al*. Gaussian 16, Revision C.01, Gaussian, Inc., Wallingford, CT, **2016**.
[24] D. Ma and L. Duan, *Chem. Rec*., **2019**, *19*, 1483.
[25] F.-C. Zhao, Z.-Q. Zhang, Y.-P. Liu, Y.-F. Dai, J.-S. Chen and D.-G. Ma, *Org. Electron.*, **2012**, *13*, 1049.
[26] P. Tao, Z. Lv, F.-Q. Zhao, X.-K. Zheng, H. Jiang, W. Li, Y. Deng, S. Liu, G. Xie, W.-Y. Wong and Q. Zhao, *Inorg. Chem.*, **2023**, *62*, 1202.